ANALYSIS OF PARTICLE DEPOSITION FROM TURBULENT LIQUID-FLOW ONTO SMOOTH CHANNEL WALLS

Magali Dupuy, Arunvady Xayasenh, Emmanuel Waz, Pierre Le Brun, Hervé Duval

ANALYSIS OF PARTICLE DEPOSITION FROM TURBULENT LIQUID-FLOW ONTO SMOOTH CHANNEL WALLS

Magali DUPUY[1*], Arunvady XAYASENH[1], Emmanuel WAZ[2], Pierre LE BRUN[2], Hervé DUVAL[1]

[1] Laboratory of Chemical Engineering and Materials, École Centrale Paris, 92295 Châtenay-Malabry, FRANCE

[2] Constellium, Voreppe Research Centre, CS 10027, 38341 Voreppe Cedex, FRANCE

* E-mail: magali.dupuy@ecp.fr

ABSTRACT

In this study, we analyse the motion of hydrosol particles in the near-wall shear layer of a turbulent channel flow. The liquid flow-field is described using the kinematic model proposed by Fan and Ahmadi (1995) combined with Lagrangian particle tracking. Numerical simulations were performed for friction velocity ranging from 1.5 mm.s^{-1} to 15 mm.s^{-1}, particle diameter from 5 to 50 µm, particle to liquid density ratio from 1 to 1.4 and wall roughness height from 0.1 to 1µm. The results show that the inertia effects are very weak. For nonbuoyant particles, direct interception is the main deposition mechanism and a law giving the deposition velocity as a function of the different parameters is proposed. For buoyant particles the deposition is controlled by sedimentation for the smallest values of friction velocity. When friction velocity increases, the direct interception contribution increases as well, and may prevail on sedimentation.

Keywords: Fouling/clogging, metal refining, turbulent deposition, Lagrangian methods, liquid aluminum.

NOMENCLATURE

Greek Symbols

δ Distance from particle surface to wall, [m].
ρ Mass density, [kg.m^{-3}].
τ_p Relaxation time, [s].
τ_p^+ Stokes number.
μ Dynamic viscosity, [kg.m^{-1}.s^{-1}].
ν Cinematic viscosity, [m^2.s^{-1}].
σ_w Shear stress at the wall, [kg.m^{-1}.s^{-2}].

Latin Symbols

C_0 Mean particle concentration, [m^{-3}].
D Domain length, [m].
d Diameter, [m].
e Shift in the velocity profile at the wall, [m].
f Friction coefficient.
F Force.
F_D Drag force.
F_L Lift force.
g Gravity, [m.s^{-2}].
J Particle mass transfer rate, [m^{-2}.s^{-1}].
k Roughness height, [m].
l^* Characteristic length scale at the solid wall, [m].
r_p Particle radius, [m].
t^* Characteristic time scale at the solid wall, [s].
u Velocity, [m.s^{-1}].
u^* Characteristic velocity at the solid wall, [m.s^{-1}].
V_d Deposition velocity, [m.s^{-1}].
V_s Sedimentation velocity, [m.s^{-1}].
y_c Capture distance, [m].
z_p Distance from particle center to wall, [m].

Suberscripts

d Deposition.
D Drag.
f Fluid.
l Limiting trajectory.
L Lift.
p Particle.
s Sedimentation.
w Wall.
$\parallel$ Parallel to the wall.
$\perp$ Perpendicular to the wall.

Superscripts

$+$ Dimensionless quantity.
$*$ Value at the solid wall.

INTRODUCTION

In aluminum industry, the elimination of inclusion is of great importance because the quality and properties of the aluminum products rely on it. Indeed, the presence of inclusions may lead to decohesion on forged products or tearoff during forming with high plastic deformation such as extrusion or rolling (Duval *et al.* 2009). It can also have a pernicious influence on fatigue properties, as many studies have shown (El-Soudani and Pelloux 1973, Jordon *et al.* 2010, Tijani *et al.* 2013, Tiryakioğlu 2009). That is why some processing operations are dedicated to removing inclusions from the liquid aluminum. Many studies have been conducted to estimate and improve the efficiency of such processes,

such as purification by flotation (Mirgaux *et al.* 2009), filtration with ceramic foam filters (Acosta and Castillejos 2000 I and II, Duval *et al.* 2009, Zhou *et al.* 2003), filtration with ceramic particle with active coatings (Zhou *et al.* 2003), or filtration with electromagnetic field (He *et al.* 2012, Natarajan and El-Kaddah 2002, Xu *et al.* 2007).

Metal processing often include transporting liquid metal from one apparatus to another thanks to a trough. This step might affect the inclusion content (advantageously or not) and is not yet accurately described. The present study attempts to give more insight about deposition of inclusions at the solid bottom wall of a trough carrying liquid aluminum. Even though deposition on solid walls has been widely studied for aerosol (Fan and Ahmadi 1993, Tian and Ahmadi 2007, Guha 1997, Lai 2005, Narayanan *et al.* 2003, Zhao and Wu 2006) it remains hardly ever investigated in the case of suspended particles in a liquid *i.e.* hydrosol. A hydrosol differs from an aerosol by its solid to fluid density ratio of the order of 1 whereas an aerosol is characterized by a large density ratio, *i.e.* about 10^3. Hydrosol turbulent deposition is addressed in this paper, by means of numerical simulations.

The following sections start with the description of the particle deposition model. Then the model is applied to the deposition of non-buoyant as well as buoyant inclusions. The influence on deposition of different parameters, such as the particle diameter or the inclusion to liquid density ratio for instance, is investigated. The main purposes of this paper are (i) to identify and quantify the deposition mechanisms, (ii) to establish the suitable kinetic laws for inclusion turbulent deposition in liquid aluminum.

MATHEMATICAL MODEL

The trough is modelled as an open rectangular channel. The present study focuses on the inclusion deposition on the horizontal solid bottom wall of the channel (figure 1). Inclusions can be transported by the turbulent liquid metal flow from the center of the channel to the bottom wall where they may be captured. Since we are interested in deposition, the turbulent flow field is not solved in the whole height of the channel but in a zone of interest close to the deposition wall (figure 1). Inside this zone of interest the flow field is described by the analytical sublayer model of Fan and Ahmadi (1995) and the inclusion trajectories are computed by Lagrangian particle tracking using an in-house CFD code.

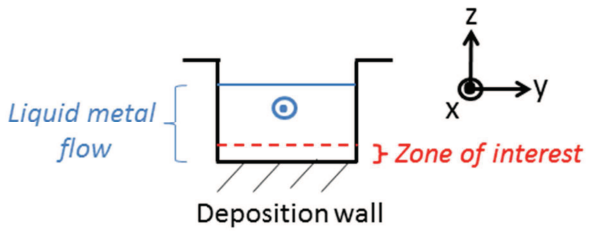

Figure 1: Configuration of liquid metal flow in a channel, with deposition at the channel bottom wall.

It is possible to determine a characteristic fluid velocity at the solid wall, called the friction velocity u^* and defined as

$$u^* = \sqrt{\frac{\sigma_w}{\rho_f}} \quad (1)$$

where $\sigma_w = \mu_f \, \partial u_{fx}/\partial z$ is the shear stress at the wall. Thanks to the characteristic velocity at the solid wall u^* it is possible to define characteristic time and length scales, t^* and l^* respectively, such as

$$t^* = \frac{\nu_f}{(u^*)^2} \quad (2)$$

$$l^* = \frac{\nu_f}{u^*} \quad (3)$$

These characteristic scales are used to make dimensionless the model parameters, which are then labeled with a $^+$ exponent.

Inclusion capture at the wall

As far as deposition is concerned, it is assumed that once there is a direct contact between the inclusion and the wall, the deposition process is completed with no rebound effect included. The solid wall is supposed to be smooth. Therefore the distance of capture y_c is defined as

$$y_c^+ = r_p^+ \quad (4)$$

Small wall roughness height k can be included in the model. The wall roughness modifies the capture height y_c^+ which becomes

$$y_c^+ = r_p^+ + k^+ - e^+ \quad (5)$$

with $k^+ = ku^*/\nu_f$ the dimensionless roughness height and e the shift in the velocity profile at the wall induced by the presence of the roughness. Its value is given by the model by Zhao and Wu (2006) such as

$$\frac{e^+}{k^+} = \begin{cases} 0 & \text{if } k^+ < 3 \text{ (hydraulically smooth)} \\ \left.\begin{array}{ll} 0.3219\ln(k^+) - 0.3456 & \text{if } 3 < k^+ < 30 \\ 0.0835\ln(k^+) - 0.4652 & \text{if } 30 < k^+ < 70 \end{array}\right\} & \text{(transition)} \\ 0.82 & \text{if } k^+ > 70 \text{ (completely rough)} \end{cases} \quad (6)$$

The configurations computed in the present study are hydraulically smooth.

Liquid metal turbulent flow

Many experimental and numerical studies have been carried out in order to investigate the flow field behavior in the turbulent boundary layer at a wall as well as the turbulent deposition at a solid wall (Cleaver and Yates 1975, Corino and Brodkey 1969, Kim *et al.* 1971, Kline *et al.* 1967, Smith and Metzler 1983). It has been found that the particles are conveyed to the wall by the fluid vortices close to the deposition wall. These eddies are organized with burst and sweep structures in the viscous sublayer ($z^+ < 10$) and the buffer layer ($10 \leq z^+ < 30$) (Kim *et al.* 1971). Fan and Ahmadi (1995) have proposed to model these structures by a frozen flow field, such as

$$u_f^+ = \begin{cases} u_{fx}^+ = \frac{1}{0.075}\tanh(0.075z^+) \\ u_{fy}^+ = \frac{11}{16}\left(\frac{2A}{\Lambda^+}\right)\left(\frac{2z^+}{\Lambda^+}\right)^{-5/16}\sin\left(\frac{2\pi z^+}{\Lambda^+}\right)\sin\left(\frac{2\pi y^+}{\Lambda^+}\right) \\ \quad + A\left(\frac{2\pi}{\Lambda^+}\right)\left(\frac{2z^+}{\Lambda^+}\right)^{11/16}\cos\left(\frac{2\pi z^+}{\Lambda^+}\right)\sin\left(\frac{2\pi y^+}{\Lambda^+}\right) \\ u_{fz}^+ = -A\left(\frac{2\pi}{\Lambda^+}\right)\left(\frac{2z^+}{\Lambda^+}\right)^{11/16}\sin\left(\frac{2\pi z^+}{\Lambda^+}\right)\cos\left(\frac{2\pi y^+}{\Lambda^+}\right) \end{cases} \quad (7)$$

where $\Lambda^+ = 100$ is the dimensionless mean distance between two bursts and $A = 34{,}7$ is a constant obtained by matching the downward velocity component u_{fy}^+ given by equation (7) to a characteristic downward velocity in turbulent boundary layer flow (Fan and Ahmadi 1995). The structure of the fluid velocity field obtained from equations (7) is depicted in figure 2.

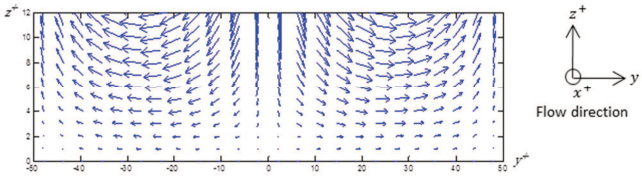

Figure 2: Fluid velocity vector field in the zone of interest (see fig.1) as given by the model of Fan and Ahmadi (1995).

Using the Fan and Ahmadi model to describe the fluid flow implies that the particles are carried out and captured at the wall thanks to the burst/sweep structures. It has been proven to be true for aerosol (Fan and Ahmadi 1995). In the present study it is assumed that it is true for hydrosol as well. On top of that, it is presumed that the burst/sweep structure has a longer lifetime than the particle trajectory.

It is expected that the main features of hydrosol deposition can be well-represented by this simplified fluid flow model of the near-wall turbulence structure.

Inclusion trajectory

Lagrangian particle tracking is considered under conditions of one-way coupling, that is to say that particle effects on flow as well as particle-particle interaction are not taken into account. This hypothesis is relevant as long as the particle volume fraction is lower than 10^{-6}. Particles are introduced in the domain at $z^+ = 12$ (figure 1) where the fluid flow reaches a maximum of turbulent kinetic energy production (Panton 2001). Therefore the particle concentration at $z^+ = 12$ is supposed to be homogeneous.

The dimensionless particle equation of motion is given as

$$\tau_p^+\frac{du_p^+}{dt^+} = \tau_p^+\left(1-\frac{\rho_f}{\rho_p}\right)\mathrm{g}^+ + \left(u_f^+ - u_p^+\right) + \tau_p^+\frac{\rho_f}{2\rho_p}\left(\frac{Du_f^+}{Dt^+} - \frac{du_p^+}{dt^+}\right) + \tau_p^+\frac{\rho_f}{\rho_p}\frac{Du_f^+}{Dt^+} + F_L^+ \quad (8)$$

where d_p is the particle diameter, μ_f the dynamic fluid viscosity, and ρ_p and ρ_f are, respectively, the particle density and the fluid density. Here g denotes the acceleration of gravity which is orientated towards the horizontal bottom wall, u_p is the particle velocity and u_f is the fluid velocity in the absence of the particle. $Du_f/Dt = \partial u_f/\partial t + u_f.\nabla u_f$ is the fluid acceleration at the instantaneous particle center. d/dt corresponds to the time derivative following the moving inclusion.

In Eq. (8), the left-hand side represents the particle inertial force. On the right-hand side, the terms are the gravitational force, the Stokes drag force (since the Reynolds particle number $Re_p = \rho_f\|u_p - u_f\|(d_p/2)/\mu_f$ is lower than 0.1), the added-mass force, the effects of pressure gradient of the undisturbed flow and the lift force. The expression of the lift force F_L is the "optimum" one given by Wang *et al.* (1997).

In Eq. (8), the Basset history term is neglected. Brownian diffusion is neglected as well since particle diameter is much larger than 1 µm.

When the particle is close to the deposition wall (*i.e.*, when the distance between the particle center and the wall is lower than about 10 d_p), it is possible to include the hydrodynamic interactions between the particle and the interface (*i.e.* lubrication effects) in the particle equation of motion. The lubrication effects are manifested in the drag force's deviation from the Stokes expression. Therefore they are taken into account through the introduction of the appropriate friction coefficients (Tien and Ramarao 2007) in the Stokes steady drag, such as

$$(F_D)_\parallel^+ = -\left[\left(u_p^+\right)_\parallel f_\parallel^t - \frac{1}{u^*}a^+ z_p^+ f_{1\parallel}^m - \frac{1}{u^*}b^+\left(z_p^+\right)^2 f_{2\parallel}^m\right]$$
$$(F_D)_\perp^+ = -\left[\left(u_p^+\right)_\perp f_\perp^t + \left(u_{f0}^+\right)_\perp f_{2\perp}^m\right] \quad (9)$$

where the subscript $\perp$ (resp. $\parallel$) is associated with the component perpendicular (resp. parallel) to the wall and z_p^+ is the dimensionless distance between the particle center and the solid wall. The values of the friction coefficients $f = f(\delta/d_p)$ depend on the separation distance δ between the particle and the solid wall made dimensionless by the particle diameter d_p as given by Tien and Ramarao (2007). The coefficients a and b are defined by (Tien and Ramarao 2007)

$$a^+ = -\frac{\partial\left(u_{f0}^+\right)_\parallel}{\partial z_p^+} + \frac{2\left(u_{f0}^+\right)_\parallel}{z_p^+}$$
$$b^+ = \frac{1}{z_p^+}\frac{\partial\left(u_{f0}^+\right)_\parallel}{\partial z_p^+} - \frac{\left(u_{f0}^+\right)_\parallel}{\left(z_p^+\right)^2} \quad (10)$$

It should be noted that $f \to 1$ when $\delta \to \infty$ and that the friction coefficient $f_\perp^t$ acting on the perpendicular component of the particle velocity, diverges as the reduced separation distance vanishes. Hence when lubrication effects are incorporated in the particle equation of motion, the solid wall roughness is included in the model as well. Consequently, the contact between the particle and the wall is achieved thanks to the roughness.

The particle equation of motion (8) is solved numerically using third-order Adams-Bashforth method.

The deposition velocity V_d is defined as

$$V_d = \frac{J}{C_0} \quad (11)$$

where J is the particle mass transfer rate at the wall and C_0 the mean particle concentration at $z^+ = 12$. The particle mass transfer rate J is evaluated thanks to the limiting trajectory. Indeed, there is a limiting value y_l

above which the inclusions introduced in the domain at the $z^+ = 12$ are transported outside the domain without ever reaching the solid wall. From the values of the limiting trajectory y_l, of u_{pl} the normal component of the inclusion velocity at $z^+ = 12$ and of D the domain length in the y^+ direction, the particle mass transfer rate can be estimated:

$$\mathrm{J} = \mathrm{C}_0 \left(\int_0^{y_l} \frac{u_{pl} \mathrm{dy}}{\mathrm{D}/2} \right) \quad (12)$$

In order to verify that the code is valid, it has been tested on a reference configuration for which experimental and numerous numerical data are available: simulations for the aerosol configuration of the experiment of Liu and Agarwal (1974) have been run. The deposition velocities computed were found to be in good agreement with the experimental results as well as the numerical models of Wood (1981) and Fan and Ahmadi (1993).
In the following, the numerical study actually consists of using the model of Fan and Ahmadi (1995) rethought in the case of a hydrosol.

Simulation parameters

The study focuses on the deposition of inclusions suspended in liquid aluminum. Numerical simulations have been run for different sets of parameters, with particle to liquid density ratio varying from 1 to 1.4, the particle diameter from 5 to 50 µm, the friction velocities from 1.5 to 15 mm.s^{-1}, and the wall roughness from 0.1 to 1 µm. The simulation parameters are summarized in table 1.

Table 1: Modelling conditions.

ρ_f	2360 kg. m^{-3}
ν_f	5.5085×10^{-7} m^2. s^{-1}
ρ_p/ρ_f	0.95 to 1.4
u^*	1.5 to 15 mm. s^{-1}
d_p	5 to 50 µm
k	0.1 to 1 µm

Some simulations are performed without inertia effects (resp. gravity): in this case, particle inertial force, added mass force, pressure gradient force and lift force (resp. gravitational force) are removed from Eq. (8). When inertia effects are taken into account, Faxen corrections are also included in the model. Indeed it has been found that even though not an inertia effect, Faxen corrections are of the same order of magnitude as the pressure gradient force (Maxey and Riley 1983).

RESULTS

As far as deposition on a horizontal wall is concerned sedimentation can overpower any other deposition mechanism. Thus, we have started by computing simulations without any gravity effect before including gravity in the model.

Simulations without gravity effect

As gravitational effect are not included in the results of figure 3, simulations run without inertia illustrate deposition by the direct interception mechanism (since inclusions are strictly moving along fluid flow streamlines) whereas simulations with inertia reveal the inertia impact mechanism. Figure 3 shows that the difference in deposition velocity, depending on whether inertia effects are included or not, remains small. Therefore, inertia is of no significant consequence in deposition and the only deposition mechanism is direct interception. This is consistent with the small values of the Stokes number τ_p^+ meaning that the particles have little inertia and react instantaneously to any modification of the fluid flow direction.

Results of figure 4 have been obtained without gravity nor inertia, thus depicting deposition by direct interception. It can be seen in figure 4 that the greater the friction velocity u^*, the more efficient the direct interception mechanism. These results actually reflect that the number of inclusion impact to the wall rises with the friction velocity. If the adhesion force between the inclusion and the wall is strong enough it will increase the deposition velocity. Nevertheless, in practice it can be suspected that if the greater the friction velocity, the more important the inclusion resuspension. Therefore, if this effect was taken into account in the present modelisation it could lessen the deposition velocity.
Figure 4 reveals that the roughness height has little effect on the deposition of the larger inclusions. On the other hand, it helps the deposition of the smallest particles. It can be concluded that the contact between the inclusion and the wall is more easily achieved when the roughness height represents a sufficient percentage of the inclusion diameter (typically when $k \geq 5\% d_p$).

The figure 5 shows that the numerical results for deposition by direct interception align well onto a curve. It is then possible to obtain a law giving the dimensionless deposition velocity by direct interception as a function of the particle diameter, the roughness height and the friction velocity as given by:

$$V_d^+ = 10^{-3} \left(\frac{d_p + 2k}{l^*} \right)^{1.7} \quad (13)$$

The effects of lubrication on direct interception have been investigated in figure 6. It is found that lubrication significantly reduces the deposition. Its effect is stronger as the roughness height is smaller. Indeed, roughness cuts off the lubrication effects which are stronger at short distance from the wall and can delay or even prevent the inclusion deposition. Nevertheless, for larger roughness height, such as those encountered in industrial processes (*i.e.* $k \gg 1$ µm), it can be expected that lubrication has no significant influence on deposition.

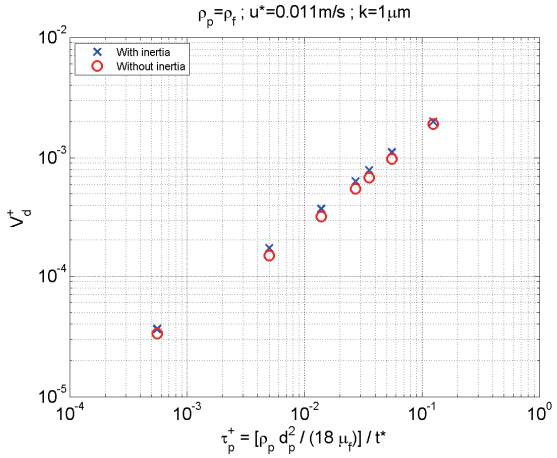

Figure 3: Dimensionless deposition velocity as a function of the inclusion Stokes number. Simulations without gravity.

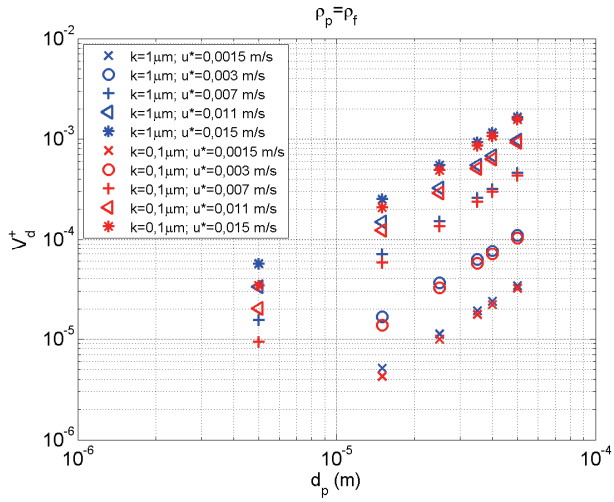

Figure 4: Dimensionless deposition velocity as a function of the inclusion diameter. Simulations without gravity nor inertia.

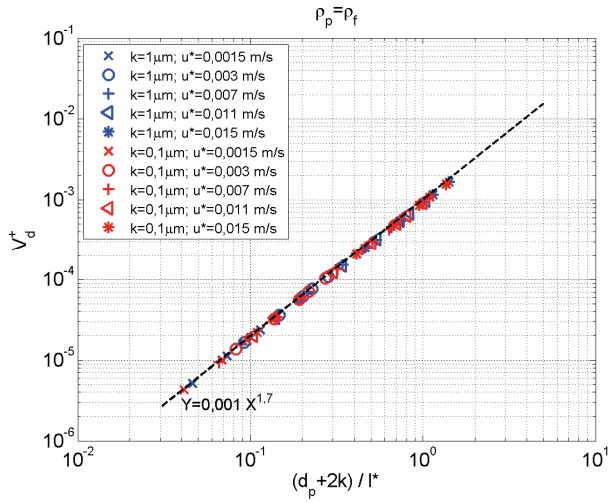

Figure 5: Dimensionless deposition velocity as a function of the inclusion diameter and the roughness height. Simulations without gravity nor inertia.

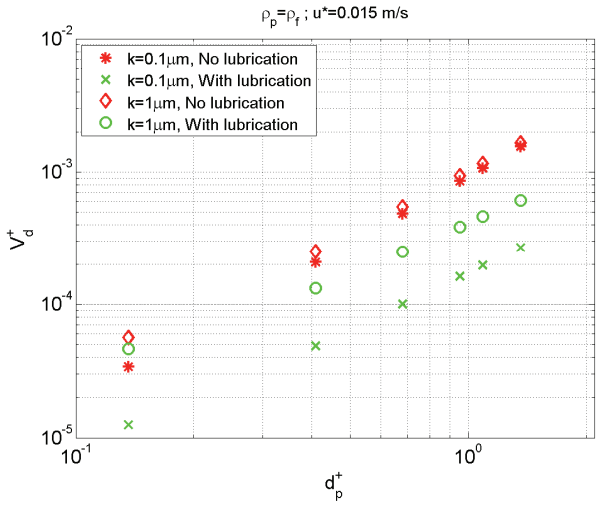

Figure 6: Dimensionless deposition velocity as a function of the dimensionless inclusion diameter. Simulations without gravity nor inertia.

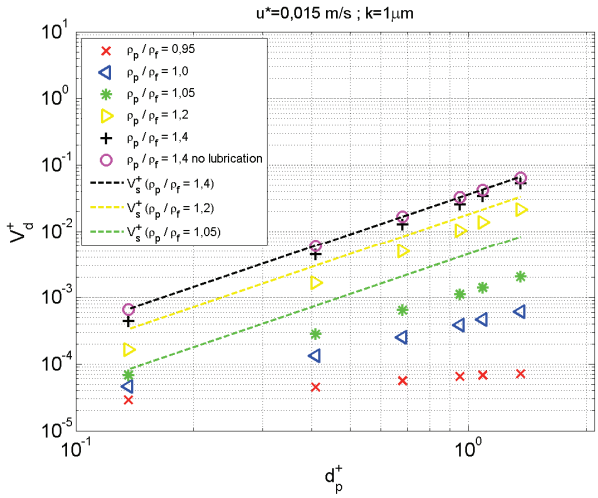

Figure 7: Dimensionless deposition velocity for different values of ρ_p/ρ_f. Simulations with lubrication.

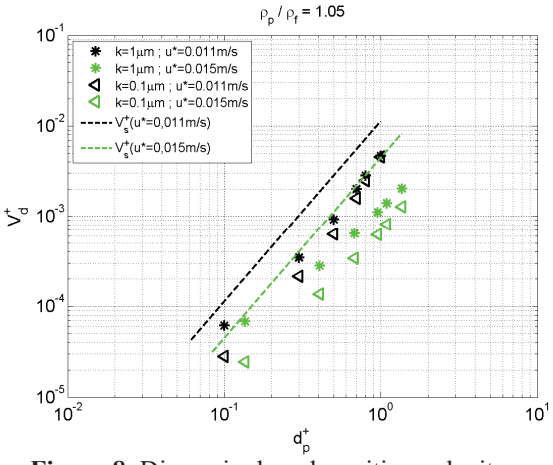

Figure 8: Dimensionless deposition velocity as a function of the dimensionless inclusion diameter. $\rho_p/\rho_f = 1.05$

Simulations with gravity effect

Configurations for which gravity is taken into account are investigated in figure 7 for different values of ρ_p/ρ_f. Figure 7 shows that for given values of friction velocity u^* and roughness height k, gravity goes against deposition for inclusion density smaller than the fluid one. On the other hand, gravity works in favour of the deposition if the inclusion density is greater than the fluid one. In that case, the greater the inclusion density compared to the fluid density, the closer to sedimentation velocity the deposition velocity. Hence it can be concluded that the sedimentation is the main deposition mechanism for inclusion dense enough compared to the fluid.
Figure 7 also shows that lubrication can reduce deposition compared to a configuration without lubrication. Nevertheless the reduction remains negligible, unlike for non-buoyant inclusions.

Unlike when $\rho_p/\rho_f > 1.2$, figures 7 and 8 show that for inclusions for which density is close to the fluid density (*i.e.* $0.95 \leq \rho_p/\rho_f \leq 1.2$), the deposition velocity significantly differs from the sedimentation velocity. It demonstrates that in that case sedimentation is not the main deposition mechanism. Figure 8 also points out that the difference between deposition velocity and sedimentation velocity grows bigger as u^* rises. Indeed, direct interception contribution on deposition increases with u^*. It can be concluded that for inclusion density larger than fluid density, sedimentation is cooperating with the direct interception mechanism and the balance between the two contributions depends on the value of ρ_p/ρ_f and u^*. As the two mechanisms react to lubrication and roughness height with different intensities as ρ_p/ρ_f and u^*vary, it becomes difficult to extract a general law that faithfully transposes the deposition velocity when $\rho_p/\rho_f \sim 1$.

CONCLUSION

Particle deposition onto a channel bottom smooth wall has been studied. Liquid aluminum flow has been obtained thanks to the sublayer model of Fan and Ahmadi (1995). Particle trajectories have been simulated by Lagrangian particle tracking under conditions of one-way coupling.
The inertia, lubrication, turbulence and wall roughness effects on deposition have been investigated.
For non-buoyant inclusions, inertia effects are not significant and the only deposition mechanism is direct interception. The higher the turbulence (*i.e.* the higher the value of u^*), the more efficient the direct interception. Wall roughness may help the deposition of the smallest inclusions. As far as direct interception is concerned, the simulated dimensionless deposition velocities (made dimensionless by the characteristic scales at the solid wall) align well onto a master curve which is a function of the particle diameter, the wall roughness and the friction velocity. On the smooth wall, lubrication has been found to significantly reduce the deposition by direct interception.

For buoyant inclusions, deposition is controlled by sedimentation for particles dense enough compared to the liquid metal. As the inclusion density gets closer to the fluid density, the sedimentation contribution on deposition decreases. On the other hand, direct interception mechanism contribution rises with $u^*$and may overcome sedimentation. As a consequence, the two mechanisms contribute to the deposition with different intensities, making it difficult to extract a general expression giving the deposition velocity for buoyant inclusions.

ACKNOWLEDGEMENTS

This research was supported by the Agence Nationale de la Recherche, as part of the PRINCIPIA project (PRocédés INdustriels de Coulée Innovants Pour l'Industrie Aéronautique, project ANR-2010-RMNP-007-01).

REFERENCES

ACOSTA G. F.A. and CASTILLEJOS E. A.H. (2000 I), "A mathematical model of aluminum depth filtration with ceramic foam filters: Part I. Validation for short-term filtration", *Metallurgical and Materials Transactions B*, **31B**, 492-502.

ACOSTA G. F.A. and CASTILLEJOS E. A.H. (2000 II), "A mathematical model of aluminum depth filtration with ceramic foam filters: Part II. Application to long-term filtration", *Metallurgical and Materials Transactions B*, **31B**, 503-514.

CLEAVER J.W. and YATES B. (1975), "A sublayer model for the deposition of particles from a turbulent flow", *Chemical Engineering Science*, **30,** 983-992.

CORINO E.R. and BRODKEY R.S.. (1969), "A visual investigation of the wall region in turbulent flow", *Journal of Fluid Mechanics*, **37,** 1-30.

DUVAL H., RIVIÈRE C., LAÉ É., LE BRUN P. and GUILLOT J.B. (2009), "Pilot-scale investigation of liquid aluminum filtration through ceramic foam filters: comparison between coulter counter measurements and metallographic analysis of spent filters", *Metallurgical and Materials Transactions B*, **40B**, 233-246.

EL-SOUDANI S.M. and PELLOUX R.M. (1973), "Influence of inclusion content on fatigue crack propagation in aluminum alloys", *Metallurgical Transactions,* **4**, 519-531.

FAN, F.G. and AHMADI, G., (1995), "Analysis of particle motion in the near-wall shear layer vortices – Application to the turbulent deposition process", *Journal of Colloid and Interface Science*, **172**, 263-277.

FAN, F.G. and AHMADI, G., (1993), "A sublayer model for turbulent deposition of particle in vertical ducts with smooth and rough surfaces", *Journal of Aerosol Science*, **24**(1), 45-64.

GUHA A. (1997), "A unified eulerian theory of turbulent deposition to smooth and rough surfaces", *Journal of Aerosol Science*, **28**(8), 1517-1537.

HE Y., LI Q. and LIU W. (2012), "Separating effect of a novel combined magnetic field on inclusions in molten aluminum alloy", *Metallurgical and Materials Transactions B*, **43B**, 1149-1155.

JORDON J.B., HORSTEMEYER M.F., YANG N., MAJOR J.F., GALL K.A., FAN. J. and McDOWELL D.L. (2010), "Microstructural inclusion influence on fatigue of a cast A356 aluminum alloy", *Metallurgical and Materials Transactions A,* **41A**, 356-363.

KIM H.T., KLINE S.J. and REYNOLDS W.C. (1971), "The production of turbulence near a smooth wall in a turbulent boundary layer", *Journal of Fluid Mechanics*, **50**, 133-160.

KLINE S.J., REYNOLDS W.C. and SCHRAUB F.A. (1967), "The structure of turbulent boundary layers", *Journal of Fluid Mechanics*, **30**, 741-773.

LAI A.C.K. (2005), "Modeling indoor coarse particle deposition onto smooth and rough vertical surfaces", *Atmospheric Environment*, **39**, 3823-3830.

MAXEY M.R. and RILEY J.J. (1983), "Equation of motion for a small rigid sphere in a nonuniform flow", *Phys. Fluids*, **26**(4), 883-889.

MIRGAUX O., ABLITZER D., WAZ E. and BELLOT J.P. (2009), "Mathematical modeling and computer simulation of molten aluminum purification by flotation in stirred reactor", *Metallurgical and Materials Transactions B,* **40B**, 363-375.

NARAYANAN C., LAKEHAL D., BOTTO, L. and SOLDATI A. (2003), "Mechanisms of particle deposition in a fully developed turbulent open channel flow", *Physics of Fluids*, **15**(3), 736-775.

NATARAJAN T.T. and El-KADDAH N. (2002), "A new method for three-dimensional numerical simulation of electromagnetic and fluid-flow phenomena in electromagnetic separation of inclusions from liquid metal", *Metallurgical and Materials Transactions B,* **33B**, 775-785.

PANTON R.L. (2001), "Overview of the self-sustaining mechanisms of wall turbulence", *Progress in Aerospace Sciences*, **37**, 341-383.

SMITH C.R. and METZLER S.P. (1983), "The characteristics of low-speed streaks in the near-wall region of a turbulent boundary layer", *Journal of Fluid Mechanics*, **129**, 27-54.

TIAN L. and AHMADI G. (2007), "Particle deposition in turbulent duct flows - Comparisons of different model predictions", *Journal of Aerosol Science*, **38**, 377-397.

TIEN C. and RAMARAO B.V. (2007), "Granular filtration of aerosols and hydrosols", *Elsevier Science & Technology Books.*

TIJANI Y., HEINRIETZ A., STETS W. and VOIGT P. (2013), "Detection and influence of shrinkage pores and non-metallic inclusions on fatigue life of cast aluminum alloys", *Metallurgical and Materials Transactions A,* **44A**, 5408-5415.

TIRYAKIOĞLU M. (2009), "Relationship between defect size and fatigue life distributions in Al-7 Pct Si-Mg Alloy castings", *Metallurgical and Materials Transactions A,* **40A**, 1623-1630.

WANG Q., SQUIRES K.D., CHEN M. and McLAUGHLIN J.B. (1997), "On the role of the lift force in turbulence simulations of particle deposition", *Int. J. Multiphase Flow*, **23**(4), 749-763.

WOOD N.B. (1981), "A simple method for the calculation of turbulent deposition to smooth and rough surfaces", *Journal of Aerosol Science*, **12**(3), 275-290.

XU Z., LI T. and ZHOU Y. (2007), "Continuous removal of non-metallic inclusions from aluminum melts by means of stationary electromagnetic field and DC current", *Metallurgical and Materials Transactions A,* **38A**, 1104-1110.

ZHAO B. and WU J. (2006), "Modeling particle deposition onto rough walls in ventilation duct", *Atmospheric Environment*, **40**, 6818-6927.

ZHOU M., SHU D., LI K., ZHANG W.Y., NI H.J., SUN B.D. and WANG J. (2003), "Deep filtration of molten aluminum using ceramic foam filters and ceramic particles with active coatings", *Metallurgical and Materials Transactions A,* **34A**, 1183-1191.